

Graphical Analysis and Simplified Quantification of Striatal and Extrastriatal Dopamine D₂ Receptor Binding with [¹²³I]Epidepride SPECT

Masanori Ichise, Masahiro Fujita, John P. Seibyl, N. Paul L.G. Verhoeff, Ronald M. Baldwin, Sami S. Zoghbi, Nallakkandi Rajeevan, Dennis S. Charney and Robert B. Innis

Department of Nuclear Medicine, Mount Sinai Hospital, and University of Toronto, Toronto, Ontario, Canada; and Departments of Psychiatry, Diagnostic Radiology and Pharmacology, Yale University, and Veterans Affairs Connecticut, West Haven, Connecticut

The purpose of this study was to extend the graphical analysis of reversible tracer binding to account for labeled lipophilic metabolites (metabolites) in quantifying [¹²³I]epidepride binding to striatal and extrastriatal D₂ receptors and, additionally, to evaluate the feasibility of simplified analysis to measure the specific volume of distribution (V₃') using single-sample blood data because the tissue ratio (R_T) may be a less reliable measure of D₂ binding in the presence of metabolites.

Methods: Multilinear regression analysis (MLRA) and graphical analysis (GA) using plasma parent (P) plus metabolite (M) activities as input and time activities of receptor-free (RF, cerebellum) and receptor-containing regions (RR, striatum and temporal cortex) derived $V_3' = (\alpha_{RR}^P - \alpha_{RF}^P)$, $V_3' = (1 + \delta) (\alpha_{RR}^P - \alpha_{RF}^P)$ and $R_T = V_3' / (V_2^P + \delta V_2^M)$, where α is a regression coefficient, δ is the equilibrium area ratio of M and P, and (V_2^P/V_2^M) are the corresponding nondisplaceable distribution volumes. V₃' by simplified analysis (SA) was calculated from R_T determined without blood data and $(V_2^P + \delta V_2^M)$ with single-blood sample data. The accuracy of these three V₃' values was assessed relative to the metabolite-accounted kinetic analysis (KA) for [¹²³I]epidepride SPECT studies of 11 healthy volunteers, in which each participant had 27 scans and 30 plasma samples drawn during the 14 h after injection. **Results:** All three V₃' values (mL/g) significantly correlated with those by KA ($r \geq 0.90$) (striatum/temporal cortex: MLRA, $77.8 \pm 36.6/2.35 \pm 1.16$; GA, $98.8 \pm 34.2/4.61 \pm 1.77$; SA, $83.9 \pm 24.8/4.26 \pm 1.74$; KA, $107.6 \pm 34.4/5.61 \pm 1.84$). However, the correlation between R_T and V₃' was only moderate ($r \leq 0.65$) because of significant intersubject variability (23%) in $(V_2^P + \delta V_2^M)$. **Conclusion:** The graphical analysis can be extended to account for metabolites in measuring D₂ binding with [¹²³I]epidepride SPECT for both high and low D₂ density regions. Additionally, simplified V₃' measurements with single blood sampling are feasible and may be a practical alternative to the tissue ratio R_T because R_T suffers as a measure of D₂ binding from significant intersubject variability in the metabolite-contributed distribution volume of the nondisplaceable compartment.

Key Words: graphical analysis; [¹²³I]epidepride; dopamine D₂ receptors; SPECT quantification; metabolite correction

J Nucl Med 1999; 40:1902–1912

Received Dec. 14, 1998; revision accepted Apr. 9, 1999.

For correspondence or reprints contact: Masanori Ichise, MD, Mount Sinai Hospital, 600 University Ave., Rm. 635 Nuclear Medicine, Toronto, Ontario M5G 1X5, Canada.

Iodine-123-epidepride is a SPECT tracer that binds reversibly and with high affinity ($K_D = 20$ pmol/L) to central dopamine D₂-like receptors (designated as D₂) (1–6). Because of its high D₂ affinity and low nonspecific binding, [¹²³I]epidepride has been used as a probe for D₂ receptors not only in the striatum but also in the extrastriatal regions (4–6), where D₂ densities are 20–80 times lower than in the striatum (7,8). Extrastriatal D₂ receptors are of central interest to studies of schizophrenia and antipsychotic drug action, because the neocortex has been cogently linked to the pathophysiology and treatment (9). Therefore, the availability of techniques that allow reliable quantification of both striatal and extrastriatal D₂ receptors in vivo is essential for such studies.

There are two potential difficulties with quantitative [¹²³I]epidepride SPECT imaging (6,10). First, the use of high-affinity tracers such as [¹²³I]epidepride is needed to measure low extrastriatal D₂ binding. However, this makes tracer kinetics remarkably slow, particularly in the high-D₂-density striatum (11). Therefore, multiple scans over several hours would be required to characterize the slow kinetics of [¹²³I]epidepride. However, the long physical half-life of ¹²³I (13 h) makes this repeated scanning feasible. In fact, the use of high-affinity tracers may actually be more suited to SPECT than to PET, which uses short-lived tracers (12,13). Second, [¹²³I]epidepride produces a significant amount of labeled lipophilic metabolites in plasma (6,14), which could cross the blood–brain barrier, hence contributing to measured brain activity and complicating D₂ quantification. Both three-compartment kinetic analysis (bolus-injection paradigm) and equilibrium analyses (constant-infusion paradigm) were previously performed to account for the metabolite in quantifying [¹²³I]epidepride D₂ binding (10). The kinetic analysis requires a technically demanding nonlinear least-squares fit (NLSQ) of experimental data to derive receptor parameters. On the other hand, the equilibrium paradigm greatly simplifies measurement of receptor parameters if the metabolites are inactive at the receptor site and

are uniformly distributed in the brain. However, the equilibrium paradigm requires constant tracer infusion over 20 h, during which clearance of [¹²³I]epidepride may change, making establishment of equilibrium difficult in some participants (10). Alternatively, graphical analyses of both reversible and irreversible tracer binding have been widely used to measure tracer-binding parameters (15–17). These techniques do not require NLSQ or constant tracer infusion, and the simplicity of the calculation greatly facilitates the comparison of experimental data.

The purpose of this study was to extend the graphical analysis to account for the metabolite in quantifying [¹²³I]epidepride binding to striatal and extrastriatal D₂ receptors in humans. These metabolites may contribute to a greater intersubject variability in the nondisplaceable distribution volume, making the tissue ratio less reliable as an outcome measure of D₂ densities (6). Therefore, the feasibility of a simplified analysis to measure the specific volume of distribution using single–blood sample data was additionally evaluated. The accuracy of these analyses was then assessed against the metabolite-accounted kinetic analysis used as a standard.

The quantification procedures for [¹²³I]epidepride presented here include the graphical, multilinear regression (MLRA), simplified and kinetic analyses. They are all based on a three-compartment tracer-kinetic model, which consists of the plasma (C₁) and intracerebral nondisplaceable (C₂) compartments (C₂ consists of free and nonspecifically bound radioactivity caused by both parent [C₂^P] and its metabolites [C₂^M] and the specifically bound receptor compartment (C₃) (Fig. 1) (Appendix A defines terms). The following assumptions are made, which are applicable to all analyses unless otherwise stated: Nonspecifically bound radioactivity in C₂ equilibrates rapidly with free-tissue radioactivity. Lipophilic compounds in plasma equilibrate rapidly with plasma protein so that the free fraction (f₁) is constant over time. The system obeys the first-order kinetics for transfer between compartments. As in the case of a close analog, remoxipride, the metabolites of [¹²³I]epidepride possess negligible affinity for D₂ receptors (18,19). Conversion of the parent to

metabolites in tissue is negligible (k₅ = 0; Fig. 1). The nondisplaceable distribution volumes of C₂^P and C₂^M in the receptor-containing tissue are identical to the corresponding distribution volumes in the receptor-free tissue, the exception being MLRA, in which the distribution volume of C₂^M can be different between the two tissues. For graphical analysis and its modifications, there exists a time t* when the system reaches transient equilibrium between the brain and plasma compartments as well as within the plasma compartment, i.e., C_b^P(t)/C_a^P(t), C_b^M(t)/C_a^M(t) and C_a^M(t)/C_a^P(t) become constant for all t > t*, where subscripts b and a denote brain and arterial plasma, respectively.

Because the system consists of two parallel input functions, C_a^P(t) and C_a^M(t), two operational equations for graphical analysis of tracer binding applicable to reversible systems proposed by Logan et al. (15) can be written as

$$\frac{\int_0^t C_b^P(t) dt}{C_b^P(t)} = \alpha^P \frac{\int_0^t C_a^P(t) dt}{C_b^P(t)} + \beta^P \text{ and} \quad \text{Eq. 1}$$

$$\frac{\int_0^t C_b^M(t) dt}{C_b^M(t)} = \alpha^M \frac{\int_0^t C_a^M(t) dt}{C_b^M(t)} + \beta^M. \quad \text{Eq. 2}$$

SPECT-measured brain radioactivity, C_b(t), represents a total of C_b^P(t), C_b^M(t) and V₁C_a(t), which cannot be separated into respective contributions, where V₁ is the plasma volume within tissue. Therefore, Equations 1 and 2 are combined to give the following two equations:

$$\frac{\int_0^t C_b(t) dt}{C_b(t)} = \alpha^P \frac{\int_0^t C_a^P(t) dt}{C_b(t)} + \alpha^M \frac{\int_0^t C_a^M(t) dt}{C_b(t)} + \beta(t) \text{ and} \quad \text{Eq. 3}$$

$$\frac{\int_0^t C_b(t) dt}{C_b(t)} = \alpha(t) \frac{\int_0^t C_a(t) dt}{C_b(t)} + \beta(t), \quad \text{Eq. 4}$$

where $\alpha(t) = \alpha^P/[1 + \delta(t)] + \alpha^M\delta(t)/[1 + \delta(t)]$, $\beta(t) = \beta^P/[1 + \theta(t)] + \beta^M\theta(t)/[1 + \theta(t)]$, $\delta(t) = \int_0^t C_a^M(t)dt/\int_0^t C_a^P(t)dt$ and $\theta(t) = C_a^M(t)/C_a^P(t)$ (Appendix B derives Eqs. 3 and 4). For all t > t*, C_b^P(t)/C_a^P(t), C_b^M(t)/C_a^M(t), $\delta(t) = \delta$ and $\theta(t) = \theta$ are constant. Equations 3 and 4 then become linear (Appendix C explains the constancy requirement). Equation 3 can be analyzed by MLRA to determine α^P , α^M or β , whereas Equation 4 can be used to find α and β as the slope and the intercept of a plot of $\int_0^t C_b(t)dt/C_b(t)$ versus $\int_0^t C_a(t)dt/C_b(t)$, respectively. The coefficients, α^P , α^M and α , represent, respectively,

$$\alpha^P = \sum_i f_1 V_i^P, \quad \text{Eq. 5}$$

$$\alpha^M = \sum_i f_1 V_i^M \text{ and} \quad \text{Eq. 6}$$

$$\alpha = [1/(1 + \delta)] \sum_i f_1 V_i^P + [\delta/(1 + \delta)] \sum_i f_1 V_i^M, \quad \text{Eq. 7}$$

where V_i^P and V_i^M are the distribution volumes (measured

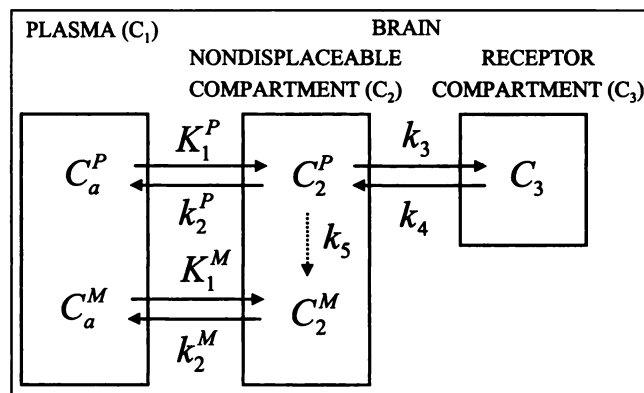


FIGURE 1. Three-compartment configuration used to model [¹²³I]epidepride kinetics, which includes labeled lipophilic metabolites. Appendix A defines terms.

against plasma water) caused by parent and metabolites, respectively, of the i^{th} compartment in a brain region.

The distribution volume of C_3 , namely $V_3 (= B'_{\text{max}}/K_D$; Appendix A), is the receptor parameter of interest and is given by MLRA and graphical analysis, respectively:

$$V_3 = (\alpha_{\text{RR}}^{\text{P}} - \alpha_{\text{RF}}^{\text{P}})/f_1 \text{ and} \quad \text{Eq. 8}$$

$$V_3 = (1 + \delta)(\alpha_{\text{RR}} - \alpha_{\text{RF}})/f_1, \quad \text{Eq. 9}$$

where the subscripts RR and RF refer to the receptor and reference regions, respectively.

Another receptor parameter often used is V_3'' because it can be measured without blood data in the absence of metabolites. V_3'' is given by

$$V_3'' = k_3/k_4 = V_3/V_2^{\text{P}} = B'_{\text{max}}/K_D V_2^{\text{P}}. \quad \text{Eq. 10}$$

In the presence of metabolites, however, V_3'' cannot be measured without blood data. If R_T is allowed to represent the specific-to-nondisplaceable tissue radioactivity ratio at equilibrium, then $R_T = V_3/(V_2^{\text{P}} + \delta V_2^{\text{M}})$ (Appendix D). From Equation 4, R_T is related to V_3'' and the slope of the graphical plot by

$$R_T = V_3/(V_2^{\text{P}} + \delta V_2^{\text{M}}) =$$

$$V_3''/(1 + \delta V_2^{\text{M}}/V_2^{\text{P}}) = \alpha_{\text{RR}}/\alpha_{\text{RF}} - 1. \quad \text{Eq. 11}$$

In deriving Equation 11, V_1 is assumed negligible (20). This R_T can be measured without blood data also using MLRA (21). The operational equation for this analysis is given by

$$\frac{\int_0^t C_{\text{RR}}(t) dt}{C_{\text{RR}}(t)} = \left(\frac{\alpha_{\text{RR}}}{\alpha_{\text{RF}}} \right) \frac{\int_0^t C_{\text{RF}}(t) dt}{C_{\text{RR}}(t)} + \left(- \frac{\alpha_{\text{RR}} \beta_{\text{RF}}}{\alpha_{\text{RF}}} \right) \frac{C_{\text{RF}}(t)}{C_{\text{RR}}(t)} + \beta_{\text{RR}}. \quad \text{Eq. 12}$$

From Equations 10 and 11, the validity of V_3'' or R_T as an outcome measure of the D_2 density hinges on the assumption that V_2^{P} or $(V_2^{\text{P}} + \delta V_2^{\text{M}})$ is the same across participants. However, the intersubject variability of $(V_2^{\text{P}} + \delta V_2^{\text{M}})$ may be potentially greater than that of V_2^{P} alone because of the additional term, δV_2^{M} . For this reason, V_3 may be considered a better outcome measure than R_T for [^{123}I]epidepride. However, the traditional measurement of V_3 requires technically demanding multiple blood sampling. On the other hand, $V_3 = R_T(V_2^{\text{P}} + \delta V_2^{\text{M}})$ can be calculated from R_T measured without blood data and separate $(V_2^{\text{P}} + \delta V_2^{\text{M}})$ determination from one-point blood and two-point SPECT data obtained at time T_1 and T_2 using the two-compartment model applied to the cerebellum as described previously (22). This method derives V_2 by the following equation:

$$V_2 = \frac{C_b(T_1)}{\int_0^{T_3} f_1 C_a(t) dt} \Gamma \left\{ \frac{C_b(T_1)}{C_b(T_2)} \right\}, \quad \text{Eq. 13}$$

where T_1 , T_2 and T_3 are arbitrary, and the function Γ is prepared for each value of $C_b(T_1)/C_b(T_2)$ by group-averaging the values of function $\Gamma = [C_b(T_3) + k_2 \int_0^{T_3} C_b(t) dt] / k_2 C_b(T_1)$. The integral input function is determined from single-blood sample data. The relationship between $C_b(T_1)/C_b(T_2)$ and k_2 is predetermined by calculating the ratio of convolution integrals of the differential equation (Appendix D) describing the two-compartment kinetics, i.e., $C_b(T_1)/C_b(T_2) = \int_0^{T_1} C_a(x) \exp[-k_2(t-x)] dx / \int_0^{T_2} C_a(x) \exp[-k_2(t-x)] dx$ (22). In this study, $C_a^{\text{P}}(t)$ was used as input function in Equation 9. This derives $V_2^{\text{x}} = V_2^{\text{P}} + \delta V_2^{\text{M}}$ (Appendix D).

MATERIALS AND METHODS

Participants

The participants were 11 healthy volunteers (6 women, 5 men; mean age 31.5 ± 9.7 y; study variables expressed as mean \pm SD). Before the [^{123}I]epidepride study, participants were given 600 mg potassium iodide orally. They all gave written informed consent. The protocols were approved by the local Human Investigation Committee.

Labeling of [^{123}I]epidepride

Labeling of [^{123}I]epidepride was performed as described previously (23). The radiochemical yield was $73.7\% \pm 7.5\%$ and the radiochemical purity was $97.8\% \pm 1.2\%$. Retrospective sterility testing was negative. The specific activity was estimated to be at least $>185,000$ GBq/mmol.

Data Acquisition

The detailed data acquisition protocols have been described previously (10). In brief, SPECT imaging was performed using a triple-headed system (Prism 3000XP; Picker International, Inc., Cleveland, OH) equipped with high-resolution fanbeam collimators (full width at half maximum 12.2 mm). Each participant received an intravenous injection of [^{123}I]epidepride (374 ± 15 MBq) over 30 s. Serial scans were acquired as follows: 4 scans for 3 min each, 4 scans for 6 min each, 7 scans for 10 min each, followed by an interval of 50–60 min during which participants were allowed to rest outside the gantry, and then multiple 20-min scans up to 13.5 ± 1.0 h after injection. To aid head repositioning and the subsequent image coregistration between scans, five radioactive fiducial markers were glued on the participants' heads to identify the canthomeatal plane. To identify anatomic brain regions, MR images were acquired using a 1.5-T unit (Sigma; General Electric Medical Systems, Milwaukee, WI) as described previously (10).

Using a peristaltic pump (2501-001; Harvard Apparatus Inc., South Natick, MA), arterial samples were obtained every 20 s for the first 2 min through a catheter inserted in the radial artery. Subsequent samples were obtained manually at 4, 6, 8, 12, 20 and 30 min and every 30–60 min, with increasing intervals at later time points, up to 12.8 ± 1.2 h after injection.

Plasma Analysis

Arterial samples were analyzed as described previously (23). There was one major lipophilic metabolite of [^{123}I]epidepride in all participants and there were two other minor metabolites, one in 1 participant and the other in 2 participants (10). Plasma protein

binding was measured in vitro by ultracentrifugation as described previously (23). The plasma free fraction (f_1) was calculated as the ratio of the filtrate to total plasma concentrations. The mean f_1 was $13.2\% \pm 5.1\%$ with one f_1 value of 27.5%. Excluding this outlier, the mean f_1 was $12.0\% \pm 2.6\%$. Because the intersubject variability of f_1 in the latter was small, we chose to measure distribution volumes against plasma as opposed to plasma water (i.e., $V' = f_1V$), thus eliminating the potential errors in the f_1 measurement.

Image Data Analysis

SPECT images were reconstructed on a 128×128 matrix using a two-dimensional Butterworth filter (order 10, cutoff frequency 0.24 cycles/pixel) after applying a ramp backprojection filter. Attenuation correction was performed by assuming uniform attenuation equal to that of water ($\mu = 0.12 \text{ cm}^{-1}$) within an ellipse drawn around the skull as identified on MRI.

Regions of interest (ROIs) were defined on the SPECT/MR coregistered transverse image and placed on all serial SPECT images after within-subject SPECT/SPECT coregistration as described previously (10). The chosen ROIs were those placed over two receptor-containing regions, the striatum (caudate and putamen, $6.2 \pm 0.9 \text{ cm}^3$) and the extrastriatal, temporal cortex (middle and inferior temporal gyri, $11.67 \pm 2.0 \text{ cm}^3$) and one receptor-free reference region, the cerebellum ($32.1 \pm 7.3 \text{ cm}^3$). Activities (cpm/g) were averaged for each ROI and between right and left sides, were decay corrected to the time of injection and were expressed as Bq/g using a calibration factor of 45.5 Bq/cpm (10). No attempts were made to correct for partial volume or scatter effects.

Quantification of D_2 Binding

D_2 binding of [^{123}I]epidepride was determined as follows: (a) MLRA (Eq. 3) to estimate V_3' ; (b) graphical analysis (Eq. 4) to estimate V_3' and R_T , respectively; and (c) simplified analysis to estimate V_3' from R_T determined without blood data (Eq. 12) plus $V_2^{X'}$ determined with single-blood sample data (Eq. 13). To validate these analyses, the V_3' values were compared with those obtained by another independent kinetic analysis technique as described previously (10). $C_a^p(t)$ was used as input function in this kinetic analysis. The V_3' calculated by this analysis does not require a metabolite-correction factor because metabolites are assumed noncontributory to D_2 binding. However, this kinetic analysis derives an apparent nondisplaceable volume of distribution as $V_2^{X'} = V_2^{P'} + \delta V_2^{M'}$ (Appendix D). The $V_2^{X'}$ in receptor region was constrained to that in the cerebellum.

In the MLRA, including the one used to estimate R_T without blood data, time t^* was identified by plotting observed versus predicted values of the dependent variable by the MLRA (left side of Eq. 3 or Eq. 12) initially including all data points. Then, the analysis was repeated using only those data points for which $t \geq t^*$. In the preliminary MLRA evaluation using the least-squares estimation procedure, the point estimate of regression coefficients for Equation 3 was unstable. Therefore, the method of ridge estimator, which is a linear transformation of the least-squares estimator, was used instead (24). This MLRA procedure resulted in more stable estimation of the coefficient than did the least-squares estimation. The biasing parameter in the ridge regression was guided by the methods described previously (24,25). MLRA using Equation 12 for R_T was stable with the traditional least-squares estimation. In the graphical analysis, after identifying time t^* on the graphical plot, the slope was determined by simple linear regres-

sion analysis. In all regression analyses, identifiability of regression coefficients was assessed by examining the SE of the respective coefficient expressed as percentage of estimate (SEE) (26), which was then propagated to give SEE values on the outcome measures.

In the simplified analysis to calculate $V_2^{X'}$, a T_1 of 60 min, T_2 of 180 min and T_3 of 120 min were chosen. Examination of the correlation between $\int_0^{120} C_a^p(t)dt$ and the parent activity in each single sample at selected times between 1 and 360 min yielded the best linear correlation ($r = 0.91$, $P < 0.0001$) at 60 min, which was hence chosen as the optimal time for single blood sampling. To validate this simplified measurement of $V_2^{X'}$, the values of $V_2^{X'}$ were compared with those obtained independently by MLRA and graphical analysis, in which $V_2^{X'}$ was calculated from the relationships $V_2^{X'} = V_2^{P'} + \delta V_2^{M'}$ and $V_2^{X'} = (1 + \delta)\alpha_{RF}$, respectively. The errors of simplified V_3' measurements against those of graphical V_3' were evaluated by calculating the variability, defined as absolute values of the difference between the two sets of values expressed as percentage of the sum of the two. Finally, to determine the minimum duration of SPECT scanning needed to derive stable measurements of V_3' , graphical and simplified V_3' values were measured using data corresponding to increasing lengths of experiment from 60 min to the end of each experiment. The stable V_3' values were defined as those within $\pm 10\%$ of the final values using all data points.

Statistical Analysis

Two-tailed Student t tests for paired samples were performed to compare outcome measures between different analyses. The relationships of outcome measures between different analyses as well as the relationships between different outcome measures were determined by linear regression analysis. All analyses were implemented in STATISTICA (StatSoft, Inc., Tulsa, OK) except for the calculation of convolution integrals, which was implemented in SCIENCE (MicroMath Scientific Software, Salt Lake City, UT). Statistical significance was defined as $P < 0.05$.

RESULTS

Plasma Activity

The mean lipophilic metabolite activity of [^{123}I]epidepride in plasma steadily increased after injection, reaching a peak at 30 min, and then declined at a rate similar to that of parent (Figs. 2A and B). The mean percent metabolite activity was $33\% \pm 9\%$ at 30 min, $40\% \pm 13\%$ at 180 min, $42\% \pm 15\%$ at 360 min and $51\% \pm 16\%$ at 630 min. The mean $1/[1 + \delta(t)]$ and $1/[1 + \theta(t)]$ values were both close to 1 initially. The former ratio decreased quickly to 0.75 ± 0.09 at 120 min and remained constant until 840 min within 12% of the final value, whereas the latter ratio slowly decreased to 0.55 ± 0.13 at 400 min and remained constant thereafter within 15% of the final value (Fig. 2C). In contrast, both $[1 + q\delta(t)]/[1 + \delta(t)]$ and $[1 + q'\theta(t)]/[1 + \theta(t)]$ became constant more quickly the closer the values of q and q' were to unity. Examples of the time course of these ratios with differing values of q and q' are illustrated in Figure 2C. For example, when q or $q' = 0.75$, these ratios became constant at 20 min onward within 10% of the respective final values. The values of $\delta(t)$ averaged over the last five sampling points were used as the values of δ (0.59 ± 0.40).

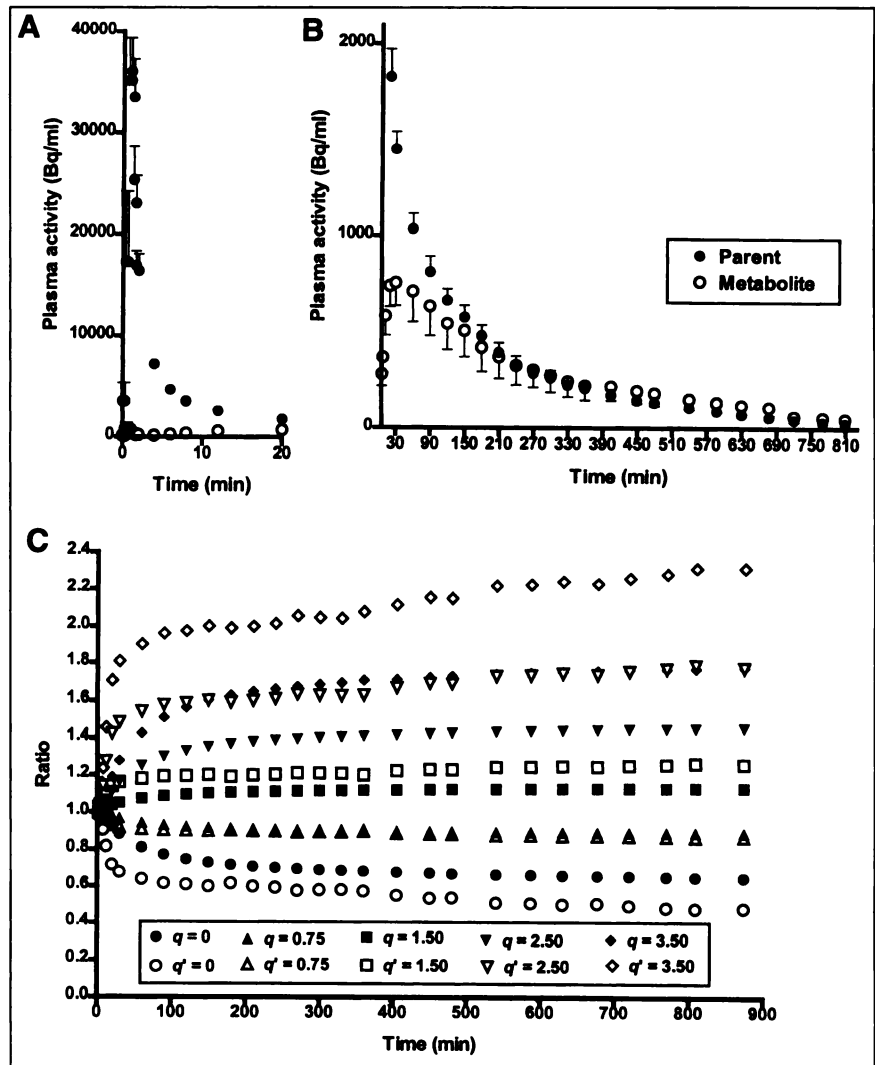


FIGURE 2. Mean arterial input function for [¹²³I]epidepride (n = 11) from 0 to 20 min (A) and 20 to 820 min (B) after injection and plots to illustrate time course of mean $[1 + q\delta(t)]/[1 + \delta(t)]$ and $[1 + q'\theta(t)]/[1 + \theta(t)]$ ratios (C), shown in solid and open symbols, respectively, when values of q or q' are 0, 0.75, 1.50, 2.50 and 3.50. Error bars in A and B indicate SD.

Brain Activity

Selected brain time-activity curves from participant 11 are shown in Figure 3. Striatal radioactivity slowly increased, reaching a peak at 238 ± 115 min, and then gradually decreased over the next several hours. The peak striatal uptake was 2.4 ± 0.4 times higher than that of cerebellum or temporal cortex. Meanwhile, radioactivity in the cerebellum and the temporal cortex both increased rapidly, reaching a peak at 5 ± 2 min and 18 ± 15 min, respectively, and then decreased more rapidly than striatal radioactivity, with the decreases being larger for cerebellum than temporal cortex. Selected SPECT images are shown in Figure 4.

Quantification of D₂ Binding

Time t* was well identified for both MLRA and graphical analyses, at 190 ± 50 min for striatum, 45 ± 10 min for temporal cortex and 30 ± 7 min for cerebellum (Figs. 5A–C). By MLRA (Eq. 3), the regression coefficients were reasonably well identified with the mean SEE of $27\% \pm 10\%$, except for striatal α^M , which was very poorly identified

(SEE $140\% \pm 90\%$). On the other hand, the identifiability of simple regression coefficients (Eq. 4) was excellent (SEE $1.1\% \pm 0.6\%$). Individual values of V_3' and R_T by different analyses are shown in Table 1.

In the striatum, the mean V_3' values by MLRA (77.8 ± 36.6 mL/g, SEE $34.6\% \pm 8.7\%$) and graphical analysis (98.8 ± 34.2 mL/g, SEE $2.1\% \pm 0.8\%$) underestimated those by kinetic analysis (107.6 ± 34.4 mL/g, SEE $4.6\% \pm 0.6\%$) by 28% and 8%, respectively. However, there were excellent correlations between MLRA/graphical analyses and kinetic analyses of V_3' values ($r = 0.93/0.98$, $P < 0.0001$) (Fig. 6A). In the temporal cortex, the mean V_3' values by MLRA (2.35 ± 1.16 mL/g, SEE $52.1\% \pm 16.3\%$) and graphical analysis (4.61 ± 1.77 mL/g, SEE $1.9\% \pm 1.4\%$) underestimated those by kinetic analysis (5.61 ± 1.84 mL/g, SEE $7.0\% \pm 2.0\%$) by 58% and 18%, respectively. However, there were also excellent correlations between MLRA/graphical analysis and kinetic analysis V_3' values ($r = 0.94/0.96$, $P < 0.0001$) (Fig. 6B). Thus, the MLRA/graphical V_3' s correlated very well with those by

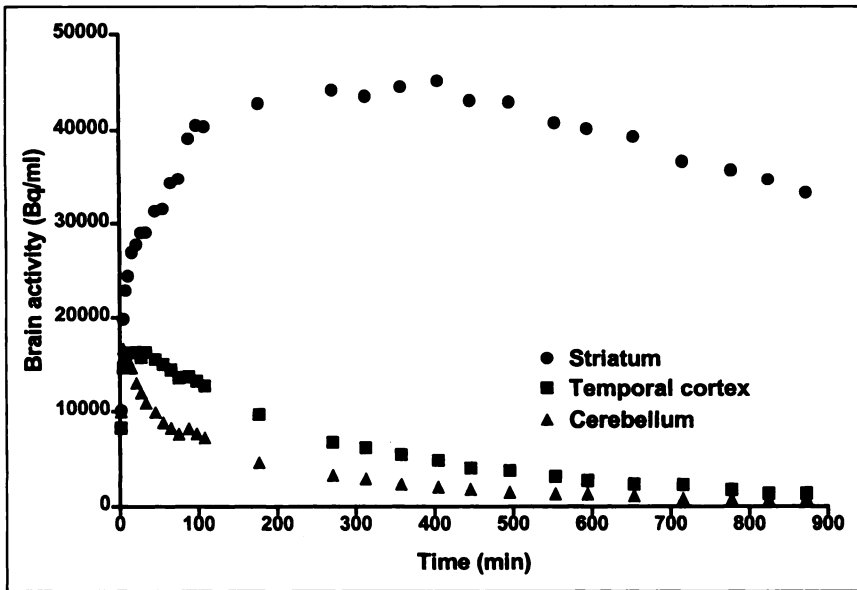


FIGURE 3. Brain time-activity curves of participant 11 after bolus administration of [¹²³I]epidepride. Striatal activity (●) reached peak at 220 min and decreased gradually thereafter, whereas activity in both temporal cortex (■) and cerebellum (▲) reached peak much earlier at 4.5 and 15 min, respectively, and decreased rapidly thereafter. These decreases were greater for cerebellum than temporal cortex.

kinetic analysis for both striatal and extrastriatal regions, although V_3' was considerably less well identified by MLRA compared with graphical or kinetic analysis.

However, the degree of the correlation between R_T estimated using blood data and V_3' by kinetic analysis for both striatum and temporal cortex was only moderate ($r = 0.65$, $P = 0.03$, and $r = 0.55$, $P = 0.04$, respectively) (Figs. 7A and B). Meanwhile, by MLRA, the mean values of $V_2^{P'}$ and $V_2^{M'}$ for cerebellum were 2.81 ± 0.82 mL/g (SEE $22.5\% \pm 10.2\%$) and 6.42 ± 3.16 mL/g (SEE $20.0\% \pm 7.6\%$), respectively, and the mean $V_2^{M'}$ values for striatum and temporal cortex were 46.8 ± 27.8 mL/g (SEE $140\% \pm 90\%$) and 11.1 ± 5.2 mL/g (SEE $24.0\% \pm 9.0\%$), respectively, both of which were significantly higher than those for cerebellum ($P < 0.01$). The identifiability of R_T using

MLRA (Eq. 12) was excellent and the R_T s without and with blood data were in excellent agreement (striatum 16.2 ± 3.6 , SEE $2.6\% \pm 9.0\%$ versus 17.2 ± 4.3 , SEE $2.5\% \pm 0.8\%$, $r = 0.96$, $P < 0.00001$; and temporal cortex 0.84 ± 0.37 , SEE $0.7\% \pm 0.5\%$ versus 0.84 ± 0.37 , SEE $1.0\% \pm 0.5\%$, $r = 0.99$, $P < 0.000001$). This justified the use of R_T without blood data in the simplified V_3' calculation. The mean simplified V_3' values (striatum 83.9 ± 24.8 mL/g, and temporal cortex 4.26 ± 1.74 mL/g) underestimated those of the kinetic analysis by 29% and 24%, respectively. However, there were excellent correlations of V_3' between the simplified and kinetic analyses (striatum: $r = 0.90$, $P < 0.001$, and temporal cortex: $r = 0.95$, $P < 0.0001$) (Figs. 6A and B). The errors in simplified V_3' measurements against the graphical V_3' were striatum $9.3\% \pm 5.5\%$ and

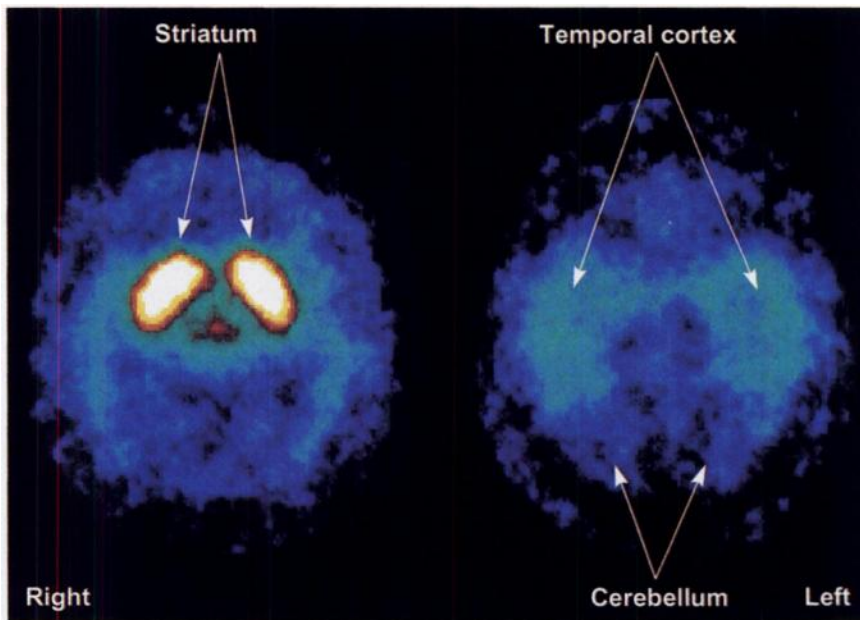


FIGURE 4. Selected transverse [¹²³I]epidepride SPECT images (summed over 51–81 min after injection in participant 1) at level of striatum (left) and inferior temporal cortex (right). High uptake is seen in striatum, whereas inferior temporal cortex shows slight but discernibly greater uptake than that in cerebellum. [¹²³I]Epidepride D_2 binding in this participant was 24 times lower in temporal cortex than in striatum.

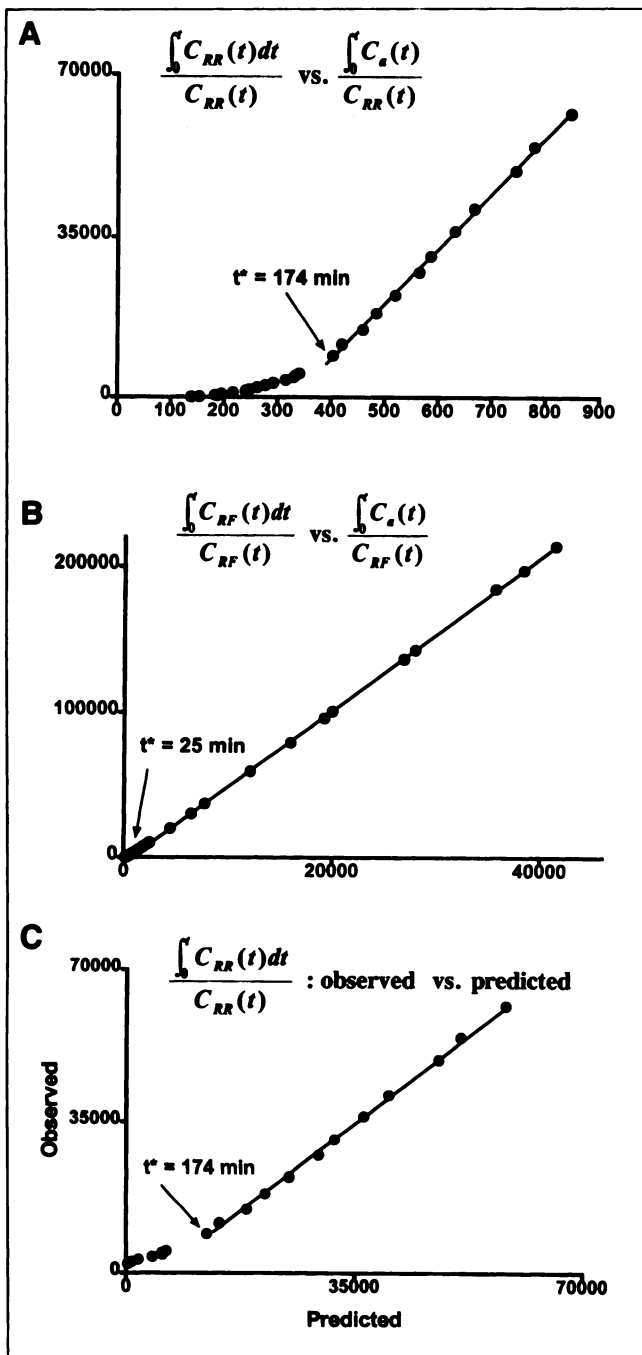


FIGURE 5. Graphical plots for striatum (A) and cerebellum (B). Graphical plot C is used to identify t^* in multilinear regression analysis to calculate R_T without blood data, which gave value of t^* identical to that of graphical plot for striatum (A). Appendix A defines terms.

temporal cortex $4.3\% \pm 1.7\%$. Therefore, the correlation of simplified V_3' with kinetic V_3' was significantly better than that of R_T with kinetic V_3' . This improvement was caused by a significant intersubject variability in V_2^M (5.25 ± 1.19 , range 2.95–6.71 mL/g, 23%). These V_2^M values were consistent with those obtained independently by MLRA/graphical analysis ($5.55 \pm 1.21/5.75 \pm 1.30$, $r = 0.91/0.93$, $P < 0.001$).

Scan Duration and Stable V_3'

Stable V_3' values were obtained with minimum scan duration of 320 ± 90 min in striatum and 220 ± 90 min for graphical analysis and 240 ± 70 min for simplified analysis in temporal cortex. Although stable graphical V_3' values were obtained with scan duration of <180 min for temporal cortex in 3 participants, the minimum scan duration for simplified analysis was 180 min by analysis design.

DISCUSSION

The graphical analysis of reversible tracer binding to [123 I]epidepride has been extended to account for its labeled metabolites. Because the D_2 affinity of the metabolite is assumed negligible, V_3' itself does not bear any contribution from metabolites. However, the nondisplaceable volume of distribution (V_2^M) includes the contribution from metabolites. Consequently, the tissue ratio R_T as an outcome measure of D_2 binding suffers from the intersubject variability of V_2^M . In fact, simple specific-to-nondisplaceable [123 I]epidepride uptake ratios at one fixed time point (3, 4 or 5 h) after injection failed to show any significant correlation with kinetic V_3' values in a previous study (10). The present alternative simplified analysis in which V_3' is derived from single sample blood data appears promising to provide a significantly improved measure of D_2 binding over R_T .

The MLRA and graphical analysis presented here are theoretically related to the methods described by Patlak et al. (27) and Mankoff et al. (28) for irreversibly binding tracers, [18 F]dopa and [11 C]thymidine, respectively, both of which incorporate a modification to the original Patlak method to account for the presence of labeled metabolites in deriving the blood-to-tissue transfer constant (K_i). The major difference between the two analyses is related to the reversible versus irreversible binding kinetics with differing outcome measures, $V_3' = K_1^P k_3 / k_2^P k_4$ versus $K_i = K_1^P k_3 / (k_2^P + k_3)$. MLRA is theoretically advantageous over the graphical analysis approach in that MLRA does not require the assumption of equal V_2^M across brain regions. Our results suggest that V_2^M is significantly higher in receptor-containing regions compared with the cerebellum. Consequently, the values of V_3' are significantly lower compared with those estimated by graphical analysis. However, both V_3' values correlated equally well with those of kinetic analysis. Considering the simplicity of the calculation as well as the superior identifiability of parameter estimates by the graphical analysis compared with MLRA, however, the former method may be preferred to the latter. Further studies using only the metabolite may be needed to clarify the validity of the assumption of equal V_2^M across brain regions.

An inherent limitation of this study design is the absence of an externally independent gold standard. An independent validation might be accomplished by performing an animal experiment designed to make a direct comparison between in vivo SPECT and in vitro epidepride binding studies using tissue samples from the same animals. Unlike in vivo

TABLE 1
 $[^{123}\text{I}]$ Epidepride D_2 Binding Measures in 11 Healthy Participants

Participant no.	V_3' (mL/g)								R_T			
	Striatum				Temporal cortex				Striatum		Temporal cortex	
	MLRA	GA	SA	KA	MLRA	GA	SA	KA	Blood data	No blood data	Blood data	No blood data
1	118.3	138.4	112.3	141.8	2.63	5.78	4.80	5.90	22.0	20.6	0.92	0.88
2	109.6	115.1	87.2	128.6	1.34	2.79	2.47	4.01	22.5	19.8	0.55	0.56
3	101.1	121.4	83.2	125.4	1.44	2.92	2.45	4.41	18.5	15.6	0.45	0.46
4	47.1	65.4	63.7	65.4	1.50	3.11	3.12	3.78	10.8	10.4	0.52	0.51
5	95.9	117.8	84.8	124.9	1.53	3.17	2.46	4.00	16.7	15.2	0.45	0.44
6	46.2	86.4	83.7	109.1	3.76	6.75	6.52	8.06	13.1	13.1	1.02	1.02
7	94.4	101.2	95.9	111.3	2.69	6.56	6.58	7.63	15.2	14.3	0.98	0.98
8	30.8	67.2	57.5	66.2	2.90	5.53	5.04	6.13	21.0	19.5	1.72	1.71
9	51.0	59.0	47.5	77.5	1.93	3.77	3.40	5.50	13.9	12.7	0.89	0.91
10	32.1	57.6	71.9	66.4	1.29	3.05	3.29	3.61	13.3	15.3	0.70	0.70
11	128.9	157.6	135.1	166.7	4.88	7.27	6.72	8.70	22.3	21.1	1.03	1.05
Mean	77.8	98.8	83.9	107.6	2.35	4.61	4.26	5.61	17.2	16.2	0.84	0.84
SD	36.6	34.2	24.8	34.4	1.16	1.77	1.74	1.84	4.3	3.6	0.37	0.37

MLRA = multilinear regression analysis; GA = graphical analysis; SA = simplified analysis; KA = kinetic analysis.

$[^{123}\text{I}]$ epidepride imaging studies, in vitro epidepride binding studies are not confounded by metabolites, cerebral blood flow or tracer clearance. Kessler et al. (7), using $[^{125}\text{I}]$ epidepride, found in six postmortem human brains the highest D_2 densities (B_{\max}) in striatum (16.6 ± 3.6 pmol/L/g) and 20–80 times lower D_2 densities in extrastriatal regions, including thalamus (1.0 ± 0.63 pmol/L/g), medial and inferior temporal cortex (0.44 ± 0.11 pmol/L/g) and frontal cortex (0.20 ± 0.03 pmol/L/g). Our mean V_3 (V_3'/f_1) values by MLRA and graphical analysis were 588 ± 249 and 767 ± 237 mL/g, respectively, in the striatum and 20 ± 11 and 38 ± 17 mL/g, respectively, in the temporal cortex, which are comparable in magnitude to their corresponding values converted to V_3 values using the mean K_D values of 22 pmol/L (striatum 756 ± 182 mL/g and temporal cortex 20 ± 5 mL/g). Regarding the absolute SPECT quantification, however, caution should be exercised because of the inherent difficulties in correcting the effects of attenuation, scatter and partial volume. Correction for the latter two effects was not implemented in this study. For example, the

thalamus, which was not our selected receptor region, has been shown to have significant D_2 binding (7). However, this low D_2 density region, which is anatomically very close to the D_2 -rich striatum, would have more significant scatter from striatum than the inferior temporal cortex.

The graphical analysis requires the constancy over time of the terms $[1 + q\delta(t)]/[1 + \delta(t)]$ and $[1 + q'\theta(t)]/[1 + \theta(t)]$. Although $1/[1 + \delta(t)]$ became constant after 120 min, $1/[1 + \theta(t)]$ became constant only after 400 min postinjection. However, the time t^* for both cerebellum and temporal cortex was <60 min. For cerebellum, the value of $q = q' = V_2^M/V_2^{P'}$ (assuming $K_1^M = K_1^{P'}$) was 2.5 ± 1.5 . Under these conditions, both $\alpha(t)$ and $\beta(t)$ can become constant before 120 min (Fig. 2C). However, these values were closer to 0 for striatum (data not shown), which partly explains why the time t^* was delayed for striatum. Logan et al. (15), in their $[N\text{-}^{11}\text{C}\text{-methyl}]\text{-}(-)\text{-cocaine}$ PET studies, have shown that the intercept β may reach its constant value before the steady state is reached. The fact that the striatal t^* was reached at

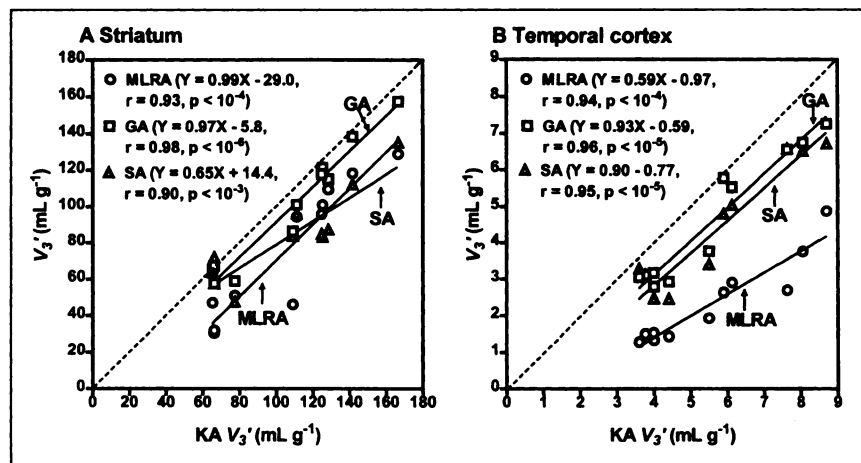


FIGURE 6. Relationships between V_3' determined by multilinear regression analysis (MLRA), graphical analysis (GA), simplified analysis (SA) and kinetic analysis (KA) for striatum (A) and temporal cortex (B). Dotted and solid lines represent line of identity with $KA V_3'$ and regression lines, respectively.

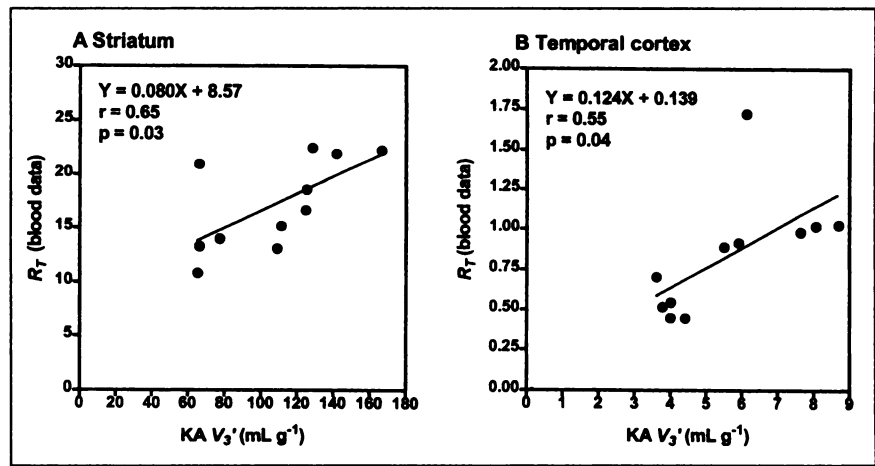


FIGURE 7. Relationships between R_T determined using blood data and kinetic analysis (KA) V_3' for striatum (A) and temporal cortex (B). Dotted and solid lines represent line of identity with KA V_3' and regression line, respectively.

190 min well before $1/[1 = \theta(t)]$ became constant at 400 min in this study suggests that the intercept for the striatal graphical plot with $[^{123}\text{I}]$ epidepride also becomes constant before the steady states are reached. On the other hand, the minimum scan duration required for obtaining stable V_3' values was not greatly different between striatum (320 min) and temporal cortex (220 min). This suggests that D_2 imaging using a high-affinity tracer may be appropriate for regions of both high and low D_2 density although experiments take several hours with $[^{123}\text{I}]$ epidepride. On the other hand, the use of a lower-affinity tracer would shorten the scan time but would require that an additional scan be obtained on a separate day.

Finally, the potential errors in simplified V_3' measurements include those arising from the use of a standard input function, estimation of $\int_0^{120} C_a^P(t)dt$ from single blood sampling and R_T measurement without blood data. Of these, probably the intersubject variability in $C_a^P(t)$ (34%) is the major source of errors; the latter two factors contribute to the overall errors to a lesser degree. The variability between estimated and true values of $\int_0^{120} C_a^P(t)dt$ was 4.1%, and between blood and no blood data, R_T s were less than 5%. The overall errors in simplified V_3' measurements were less than 10%. However, because simplified V_3' measurements were performed in the same group of participants as the one in which a standard input function was created, this method should be tested in another independent group of participants before use.

CONCLUSION

The graphical analysis can be extended to account for lipophilic metabolites in measuring D_2 binding with $[^{123}\text{I}]$ epidepride SPECT for regions of both high and low D_2 density. Additionally, simplified V_3' measurements with single blood sampling are feasible and may be a practical alternative to the tissue ratio R_T , because R_T suffers as a measure of D_2 binding from significant intersubject variability in the metabolite-contributed distribution volume of the nondisplaceable compartment.

APPENDIX A

Definitions of Terms

$C_a^P(t)$: Plasma radioactivity of parent at time t .

$C_a^M(t)$: Plasma radioactivity of metabolites at time t .
 $C_a^M(t) = \sum_i C_a^{M_i}(t)$, where $C_a^{M_i}(t)$ represents the radioactivity caused by the i^{th} metabolite.

$C_a(t)$: $C_a(t) = C_a^P(t) + C_a^M(t)$

K_1^P : Delivery kinetic rate constant for parent, which is the product of regional blood flow (F) and unidirectional extraction fraction (E).

K_1^M : Delivery kinetic rate constant for metabolites ($K_1^M = FE$), where $K_1^M = \sum_i K_1^{M_i}$ and $K_1^{M_i}$ is the kinetic constant of the i^{th} metabolite.

k_2^P, k_2^M : First-order rate constants for parent and metabolites, respectively. $k_2^M = \sum_i k_2^{M_i}$, where $k_2^{M_i}$ is the constant of the i^{th} metabolite.

k_3, k_4 : First-order rate constants between second and third compartments.

k_5 : Conversion rate constant of parent to metabolites in tissue, which is assumed to be 0.

f_1 : Free fraction of plasma parent and metabolites measured by ultracentrifugation.

B_{max} : Concentration of receptors.

B'_{max} : Concentration of receptors available for binding not occupied by tracer or intrasynaptic dopamine. B'_{max} is equal to B_{max} because $[^{123}\text{I}]$ epidepride is used at tracer doses.

K_D : Equilibrium dissociation constant for tracer-binding site complex.

$V_2^P, V_2^{P'}$: Nondisplaceable distribution volumes caused by parent, which are defined as

$$V_2^P = \frac{K_1^P}{k_2^P f_1} \text{ and } V_2^{P'} = f_1 V_2^P, \text{ respectively.}$$

$V_2^M, V_2^{M'}$: Nondisplaceable distribution volumes due to metabolites, which are defined as

$$V_2^M = \frac{K_1^M}{k_2^M f_1} \text{ and } V_2^{M'} = f_1 V_2^M, \text{ respectively.}$$

V_3, V_3' : Distribution volumes of C_3 , which are defined as

$$V_3 = \frac{B'_{\max}}{K_D} = \frac{K_1^P k_3}{k_2^P k_4 f_1} \text{ and } V_3' = f_1 V_3, \text{ respectively.}$$

V_3'' : V_3'' is defined as $V_3'' = k_3/k_4 = V_3/V_2^P = B'_{\max}/K_D V_2^P$.

R_T : Specific-to-nondisplaceable tissue radioactivity ratio at equilibrium, defined as $R_T \equiv C_{SP}(t)/C_{RF}(t) = V_3'/V_2^P$.

K_1^x, k_2^x : Delivery kinetic rate and efflux rate constants, respectively, when $C_a^P(t)$ is used as input function.

$$V_2^x, V_2'^x: V_2^x = K_1^x/k_2^x = V_2^P + \delta V_2^M \text{ and } V_2'^x = f_1 V_2^x.$$

APPENDIX B

Derivation of Equations 3 and 4

Both sides of Equations 1 and 2 are first multiplied by $C_b^P(t)$ and $C_b^M(t)$, respectively, and then these two equations were combined to give

$$\int_0^t C_b^P(t)dt + \int_0^t C_b^M(t)dt = \alpha_P \int_0^t C_a^P(t)dt + \alpha_M \int_0^t C_a^M(t)dt + \beta_P C_b^P(t) + \beta_M C_b^M(t). \quad \text{Eq. B1}$$

Divide both sides of Equation B1 by $C_b(t)$ to give Equation 3, in which the last term, $\beta(t)$, is identical to that in Equation 4. Equation 4 is obtained by the following rearrangement:

$$\frac{\int_0^t C_b(t)dt}{C_b(t)} = \left(\frac{\alpha_P \int_0^t C_a^P(t)dt + \alpha_M \int_0^t C_a^M(t)dt}{\int_0^t C_a^P(t)dt + \int_0^t C_a^M(t)dt} \right) \left(\frac{\int_0^t C_a(t)dt}{C_b(t)} \right) + \frac{\beta_P C_b^P(t) + \beta_M C_b^M(t)}{C_b^P(t) + C_b^M(t)}. \quad \text{Eq. B2}$$

Rearrange Equation B2 further to yield Equation 4.

APPENDIX C

The $\alpha(t)$ and $\beta(t)$ in Equation 4 can be written as $\alpha(t) = \alpha^P/[1 + \delta(t)\alpha^M/\alpha^P]/[1 + \delta(t)]$ and $\beta(t) = \beta^P/[1 + \theta(t)\beta^M/\beta^P]/[1 + \theta(t)]$, respectively. From these equations, it is apparent that the overall constancy requirement depends on α^M/α^P and β^M/β^P , in addition to δ and θ . These ratios can be expressed in terms of distribution volumes for the three-compartment system as $q = \alpha^M/\alpha^P = V_2^{M'}/(V_2^{P'} + V_3^{P'})$ and $q' = \beta^M/\beta^P = k_2^P/k_2^M(1 + V_3'/V_2^{P'})/[1 + k_2^P/k_4(1 + V_3'/V_2^{P'})^2]$ (14). For cerebellum and temporal cortex where V_3' is 0 or small, these ratios are not far from $\alpha^M/\alpha^P = V_2^{M'}/V_2^{P'}$ and $\beta^M/\beta^P = k_2^P/k_2^M$, respectively, and if they are not far from unity, the constancy requirement is met before δ or θ becomes constant (Fig. 2C). When they are unity, $\alpha = \alpha^P$ and $\beta = \beta^P$, which do not depend on δ or θ at all. For striatum, however, they are close to 0 because $V_3^{P'} \gg V_2^{P'}$ or $V_2^{M'}$. Therefore, the constancy requirement for $\alpha(t) =$

$\alpha^P/[1 + \delta(t)]$ and $\beta(t) = \beta^P/[1 + \theta(t)]$ depends on the terms $1/[1 + \delta(t)]$ and $1/[1 + \theta(t)]$, respectively.

APPENDIX D

The two-compartment model of a nonreceptor region with input function $C_b^P(t)$ [i.e., assuming $C_b^M(t) = 0$] is described by the following differential equation:

$$\frac{dC_b(t)}{dt} = K_1^x f_1 C_a^P(t) - k_2^x C_b(t). \quad \text{Eq. D1}$$

If $C_b^M(t)$ is included, the model is described by two equations:

$$\frac{dC_b^P(t)}{dt} = K_1^P f_1 C_a^P(t) - k_2^P C_b^P(t) \text{ and} \quad \text{Eq. D2}$$

$$\frac{dC_b^M(t)}{dt} = K_1^M f_1 C_a^M(t) - k_2^M C_b^M(t). \quad \text{Eq. D3}$$

Setting the derivatives in Equations D1–3 to 0 obtains $C_b(t')/f_1 C_a^P(t') = K_1^x/k_2^x = V_2^x$, $C_b^P(t')/f_1 C_a^P(t') = K_1^P/k_2^P = V_2^P$ and $C_b^M(t')/f_1 C_a^M(t') = K_1^M/k_2^M = V_2^M$, where t' is the time at which these derivatives are 0 or the system is in equilibrium. Noting that $C_b(t) = C_b^P(t) + C_b^M(t)$, V_2^x can be expressed as

$$V_2^x = \frac{C_b(t')}{f_1 C_a^P(t')} = \frac{C_b^P(t')}{f_1 C_a^P(t')} + \frac{C_b^M(t') C_a^M(t')}{f_1 C_a^M(t') C_a^P(t')} = V_2^P + \left[\frac{C_a^M(t')}{C_a^P(t')} \right] V_2^M = V_2^P + \delta V_2^M \quad \text{Eq. D4}$$

and

$$V_2'^x = V_2^{P'} + \delta V_2^{M'}, \quad \text{Eq. D5}$$

where δ can be derived from the steady-state principle applied to the plasma compartment (29) by the following relationship:

$$\frac{C_a^M(t')}{C_a^P(t')} = \frac{\int_0^\infty C_a^M(t)dt}{\int_0^\infty C_a^P(t)dt} = \delta. \quad \text{Eq. D6}$$

The relationship between R_T and V_2^x or $V_2'^x$ is given by

$$R_T \equiv \frac{C_{SP}(t')}{C_{RF}(t')} = \frac{C_{SP}(t')/C_a^P(t')}{C_{RF}(t')/C_a^P(t')} = \frac{V_3'}{V_2'^x} = \frac{V_3}{V_2^P + \delta V_2^M} = \frac{V_3'}{V_2^{P'} + \delta V_2^{M'}}. \quad \text{Eq. D7}$$

ACKNOWLEDGMENTS

Epidipride and its trialkylstannyl precursor were provided by Research Biochemicals International, Natick, MA, as part of the Chemical Synthesis Program of the National Institute of Mental Health, contract N01MH30003. This work was supported by funds from the Department of

Veterans Affairs (Schizophrenia Research Center) and the Public Health Science (MH30929, MH44866, DA04060) and National Institutes of Health/National Council on Radiation Risks/General Clinical Research Center program grant RR00125. The authors thank M. Early, G. Wisniewski, J. Macmullen, L. Amici, S. Giddings, Q. Ramsby and R. Feinn for excellent technical assistance. This work was presented in part at the 45th annual meeting of the Society of Nuclear Medicine, Toronto, Ontario, June 6–11, 1998.

REFERENCES

- Kessler RM, Ansari MS, de Paulis T, et al. High affinity dopamine D₂ receptor radioligands. Regional rat brain distribution of iodinated benzamides. *J Nucl Med.* 1991;32:1593–1600.
- Kessler RM, Ansari MS, Schmidt DE, et al. High affinity dopamine D₂ receptor radioligands. [¹²⁵I]epidepride, a potent and specific radioligand for the characterization of striatal and extrastriatal dopamine D₂ receptors. *Life Sci.* 1991;49:617–628.
- Joyce JN, Janowsky A, Neve KA. Characterization and distribution of [¹²⁵I]epidepride binding to dopamine D₂ receptors in basal ganglia and cortex of human brain. *J Pharmacol Exp Ther.* 1991;257:1253–1263.
- Kessler RM, Mason NS, Votaw JR, et al. Visualization of extrastriatal dopamine D₂ receptors in the human brain. *Eur J Pharmacol.* 1992;223:105–107.
- Kornhuber J, Brucke T, Angelberger P, Asenbaum S, Podreka I. SPECT imaging of dopamine receptors with [¹²³I]epidepride: characterization of uptake in the human brain. *J Neural Transm Gen Sect.* 1995;101:95–103.
- Kuikka JT, Akerman KK, Hiltunen J, et al. Striatal and extrastriatal imaging of dopamine D₂ receptors in the living human brain with [¹²³I]epidepride single-photon emission tomography. *Eur J Nucl Med.* 1997;24:483–487.
- Kessler RM, Whetsell WO, Ansari MS, et al. Identification of extrastriatal dopamine D₂ receptors in postmortem human brain with [¹²⁵I]epidepride. *Brain Res.* 1993;609:237–243.
- Hall H, Farde L, Halldin C, Hurd YL, Pauli S, Sedvall G. Autoradiographic localization of extrastriatal D₂-dopamine receptors in the human brain using [¹²⁵I]epidepride. *Synapse.* 1996;23:115–123.
- Knable MB, Weinberger DR. Dopamine, the prefrontal cortex and schizophrenia. *J Psychopharmacol.* 1997;11:123–131.
- Fujita M, Seibyl JP, Verhoeff NP, et al. Kinetic and equilibrium analyses of [¹²³I]epidepride binding to striatal and extrastriatal dopamine D₂ receptors. *Synapse.* 1999;in press.
- Laruelle M, Wallace E, Seibyl JP, et al. Graphical, kinetic, and equilibrium analyses of in vivo [¹²³I] beta-CIT binding to dopamine transporters in healthy human subjects. *J Cereb Blood Flow Metab.* 1994;14:982–994.
- Lassen NA. A reappraisal of the relative merits of SPET and PET in the quantitation of neuroreceptors: the advantage of a longer half-life [editorial]. *Eur J Nucl Med.* 1996;23:1–4.
- Ichise M, Ballinger JR. SPECT imaging of dopamine receptors [editorial]. *J Nucl Med.* 1996;37:1591–1595.
- Bergstrom KA, Halldin C, Yu MX, et al. The metabolite pattern of [¹²³I]epidepride pattern in human plasma determined with a gradient HPLC method. *J Labelled Compds Radiopharm.* 1997;40:151–153.
- Logan J, Fowler JS, Volkow ND, et al. Graphical analysis of reversible radioligand binding from time-activity measurements applied to [¹¹C-methyl]-(-)-cocaine PET studies in human subjects. *J Cereb Blood Flow Metab.* 1990;10:740–747.
- Patlak CS, Blasberg RG, Fenstermacher JD. Graphical evaluation of blood-to-brain transfer constants from multiple-time uptake data. *J Cereb Blood Flow Metab.* 1983;3:1–7.
- Gjedde A. Calculation of cerebral glucose phosphorylation from brain uptake of glucose analogs in vivo: a re-examination. *Brain Res.* 1982;257:237–274.
- Mohell N, Sallemark M, Rosqvist S, Malmberg A, Hogberg T, Jackson DM. Binding characteristics of remoxipride and its metabolites to dopamine D₂ and D₃ receptors. *Eur J Pharmacol.* 1993;238:121–125.
- Ogren SO, Lundstrom J, Nilsson LB, Widman M. Dopamine D₂ blocking activity and plasma concentrations of remoxipride and its main metabolites in the rat. *J Neural Transm Gen Sect.* 1993;93:187–203.
- Phelps ME, Huang SC, Hoffman EJ, Kuhl DE. Validation of tomographic measurement of cerebral blood volume with C-11-labeled carboxyhemoglobin. *J Nucl Med.* 1979;20:328–334.
- Ichise M, Ballinger JR, Golan H, et al. Noninvasive quantification of dopamine D₂ receptors with iodine-123-IBF SPECT. *J Nucl Med.* 1996;37:513–520.
- Odano I, Ohkubo M, Takahashi M. Quantification of cerebral blood flow and partition coefficient using iodine-123-iodoamphetamine. *J Nucl Med.* 1997;38:1248–1253.
- Baldwin RM, Zea-Ponce Y, Zoghbi SS, et al. Pharmacokinetics of the three radioiodinated dopamine D₂ receptor ligands [¹²³I]IBF, [¹²³I]epidepride and [¹²³I]2'-ISP in nonhuman primates. *Nucl Med Biol.* 1994;21:969–976.
- Montgomery SA, Peck EA. Multicollinearity. In: Montgomery SA, Peck EA, eds. *Introduction to Linear Regression Analysis.* 2nd ed. New York, NY: Wiley-Interscience; 1992:305–365.
- Hoerl AE, Kennard RW, Baldwin KF. Ridge regression: some simulations. *Commun Statist.* 1975;4:105–123.
- Ichise M, Ballinger JR, Vines D, Tsai S, Kung HF. Simplified quantification and reproducibility studies of dopamine D₂-receptor binding with iodine-123-IBF SPECT in healthy subjects. *J Nucl Med.* 1997;38:31–37.
- Patlak C, Dhawan V, Takikawa S, Chaly T, Robeson W, Eidelberg D. Estimation of striatal uptake rate constant of FDOPA using PET: methodologic issues. In: Uemura K, Lassen NA, Jones T, Kanno I, eds. *Quantification of Brain Function: Tracer Kinetics and Image Analysis in Brain PET.* Amsterdam, The Netherlands: Elsevier Science; 1993:263–268.
- Mankoff DA, Shields AF, Graham MM, Link JM, Krohn KA. A graphical analysis method to estimate blood-to-tissue transfer constants for tracers with labeled metabolites. *J Nucl Med.* 1996;37:2049–2057.
- Lassen NA. Neuroreceptor quantitation in vivo by the steady-state principle using constant infusion or bolus injection of radioactive tracers. *J Cereb Blood Flow Metab.* 1992;12:709–716.